Journal of Sound and Vibration 329 (2010) 4970–4979

Contents lists available at ScienceDirect

Journal of Sound and Vibration

journal homepage: www.elsevier.com/locate/jsvi

Modeling and performance study of a beam microgyroscope

M. Ghommem [a,*], A.H. Nayfeh [a], S. Choura [b], F. Najar [b], E.M. Abdel-Rahman [c]

[a] Department of Engineering Science and Mechanics, MC 0219, Virginia Polytechnic Institute and State University, Blacksburg, Virginia 24061, USA
[b] Applied Mechanics and Systems Research Laboratory, Tunisia Polytechnic School, BP 743, La Marsa 2078, Tunisia
[c] Department of Systems Design Engineering, University of Waterloo, Waterloo, Ontario, Canada N2L 3G1

ARTICLE INFO

Article history:
Received 27 August 2009
Received in revised form
10 June 2010
Accepted 10 June 2010
Handling Editor: S. Ilanko
Available online 1 July 2010

ABSTRACT

We develop a mathematical model of a microgyroscope whose principal component is a rotating cantilever beam equipped with a proof mass at its end. The microgyroscope undergoes two flexural vibrations that are coupled via base rotation about the microbeam longitudinal axis. The primary vibratory motion is produced in one direction (drive direction) of the microbeam by a pair of DC and AC voltages actuating the proof mass. The microbeam angular rotation induces a secondary vibration in the orthogonal (sense) direction actuated by a second DC voltage. Closed-form solutions are developed for the linearized problem to study the relationship between the base rotation and gyroscopic coupling. The response of the microgyroscope to variations in the DC voltage across the drive and sense electrodes and frequency of excitation are examined and a calibration curve of the gyroscope is obtained analytically.

1. Introduction

Inertial sensors are extensively used in automotive, military, and aerospace systems [1]. Advances in micromachining have made it possible to produce precision inertial sensors at low cost. For many of these applications, sensors are required to be cost-effective, small, and their power consumption must be suitable for battery operated devices. Micromachined devices can fulfill these requirements.

Microgyroscopes have been the subject of intensive research in the past few years [2–5]. Their objective is to measure the angular displacement or its rate of change over time. Miniaturizing these devices has advantages because conventional gyroscopes are large in size, wear out after several thousand hours of use, and are expensive. Further, miniaturized systems can be easily integrated into microelectronics.

Vibrating microgyroscopes include tuning forks, vibrating beams, and vibrating shells [1]. They work by making use of the Coriolis force. During operation, an alternating force oscillates the proof mass of the microgyroscope. When this oscillating body (drive oscillations) is placed in a rotating frame, the Coriolis force produces secondary oscillations (sense oscillations), which are orthogonal to the driven oscillations. The angular velocity of the rotating frame can be estimated by analyzing the sense oscillations [6].

Among the various kinds of microgyroscopes, suspended vibratory types are dominant because they are more suitable for batch fabrication in current micromachining processes. Miniaturized gyroscopes differ in the actuation principle (electrostatic, electromagnetic, or piezoelectric) and the transduction principle used to generate the read out signal from the sense oscillations (capacitive, piezoelectric, piezoresistive, electromagnetic, or optical). However, a large number of

* Corresponding author. Tel.: +1 540 257 4741.
E-mail address: mehdig@vt.edu (M. Ghommem).

0022-460X/$ - see front matter © 2010 Elsevier Ltd. All rights reserved.
doi:10.1016/j.jsv.2010.06.009

microgyroscopes reported in the literature use electrostatic actuation and detection [7]. The complicated dynamics and extremely small detection signals have made gyroscopes one of the most challenging devices to be realized in micromachining. In fact, electrostatic forces can induce the 'pull-in' instability where the restoring forces are unable to resist the capacitive forces, resulting in the electrodes collapsing onto each other.

A large number of sophisticated designs [8,9] have been developed to increase the sensitivity and reduce the cost of microgyroscopes. Hong et al. [10] and Jeong [11] increased the sensitivity of MEMS vibratory gyroscopes by matching the natural frequencies of the drive and sense directions and exciting the drive oscillations near resonance. Jeong [11] found that the difference in the natural frequencies of the drive and sense directions and the quality factor are the most important factors in determining the sensitivity of this type of microgyroscopes. Acar and Shkel [8] eliminated the need for matching the natural frequencies of the drive and sense direction by driving a gimbal-type torsional MEMS gyroscope at the anti-resonance frequency of the drive mode, which is designed to be equal to the resonance frequency of the sense direction.

Esmaeili et al. [12] developed the characteristic equation of a microgyroscope made of a cantilever beam and a tip mass. The beam was assumed to vibrate in two orthogonal planes subject to a base rotation about its longitudinal direction. They used the Euler–Bernoulli theory to represent the microbeam and a linear approximation to represent the electrostatic force and neglected the effects of torsion and rotary inertia. Bhadbhade and Jalili [13], and Bhadbhade et al. [14] examined coupled flexural-torsional vibrations of a beam gyroscope undergoing bending in one plane and twisting due to a rotational base motion, ignoring the rotary inertia effects. They derived the coupled governing equations of motion, solved them using an assumed mode approach, and analyzed the relationship between the base rotation and the gyroscopic coupling.

In the present work, we focus on modeling and predicting the performance of a microgyroscope consisting of a micro cantilever beam with a rigid proof mass at its end. The rigid mass is coupled to two electrodes in the drive and sense directions, which are attached to the rotating base. The microbeam is driven by an AC voltage in one direction, which induces vibrations in an orthogonal direction due to the rotation about the microbeam longitudinal axis. The electrode placed at the sense direction is then used to measure the induced motions and extract the underlying angular speed.

2. Modeling of beam microgyroscopes

The beam is attached to a moving base as shown in Fig. 1. It has a uniform square cross-section, a length L, and a mass per unit length m. A tip mass M is attached to the right end of the beam. The beam displacement is made of two bending components, $w(x,t)$ and $v(x,t)$, along the z and y directions, respectively. Equal DC voltages are applied in both directions. Hence, the beam undergoes only flexural displacements. We follow Nayfeh and Pai [15] and express the total kinetic energy as

$$K=\frac{1}{2}\int_0^L [2\Omega^2 J(v'^2+w'^2)+m(\dot{v}^2+\dot{w}^2)]\,\mathrm{d}x+\frac{1}{2}\int_0^L m[2(v\dot{w}-w\dot{v})\Omega+\Omega^2(v^2+w^2)]\,\mathrm{d}x$$
$$+\frac{1}{2}\int_0^L [J\dot{v}'^2+J\dot{w}'^2+2\Omega J(v'\dot{w}'+w'\dot{v}')]\,\mathrm{d}x+\frac{M}{2}(\dot{v}_L^2+\dot{w}_L^2+2v_L\dot{w}_L\Omega-2w_L\dot{v}_L\Omega+v_L^2\Omega^2+w_L^2\Omega^2)+LJ\Omega^2 \quad (1)$$

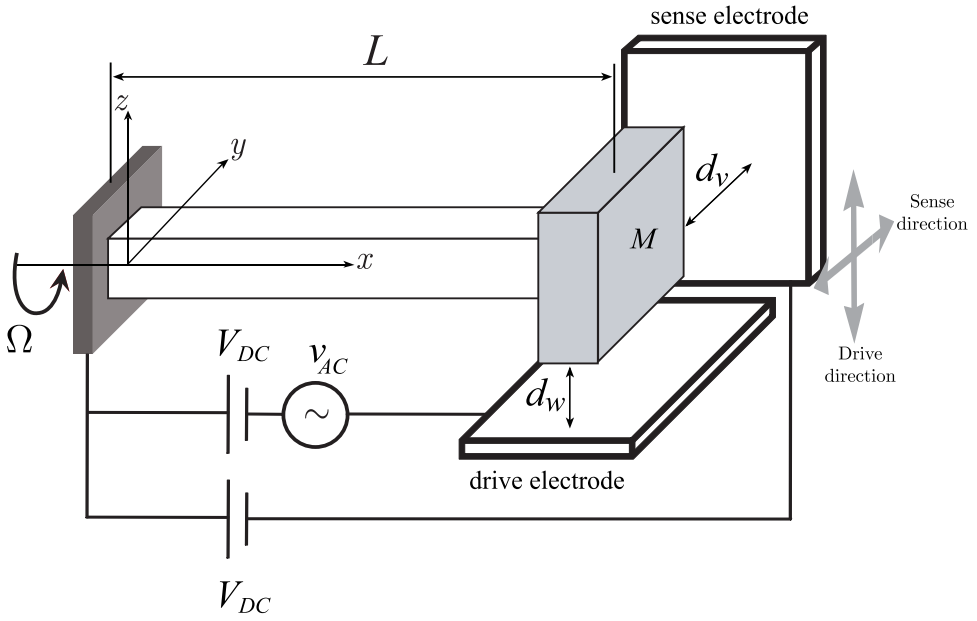

Fig. 1. Schematic of a cantilever beam with a tip mass under base rotational motion.

where $J=\int_A \rho y^2\,dA=\int_A \rho z^2\,dA$ ($m=\rho A$, $w_L=w(L,t)$, and $v_L=v(L,t)$. Here, the prime and the dot denote the derivatives with respect to x and t, respectively.

The total potential energy of the beam microgyroscope subjected to electrostatic forces in the drive and sense directions is given by

$$V=\frac{1}{2}EI\int_0^L (w''^2+v''^2)\,dx-\frac{\varepsilon A_v V_{DC}^2}{2(d_v-v_L)}-\frac{\varepsilon A_w (V_{DC}+v_{AC}(t))^2}{2(d_w-w_L)} \tag{2}$$

where (A_w,d_w) and (A_v,d_v) are the area and gap distance of the drive and sense capacitors, respectively.

The equations of motion governing the flexural vibrations of the system can be derived using Hamilton's principle

$$\int_{t_1}^{t_2}(\delta K-\delta V)\,dt=0 \tag{3}$$

This leads to the equations of motion

$$EIv^{iv}-mv\Omega^2+2Jv''\Omega^2-2m\dot{w}\Omega+m\ddot{v}-mw\dot{\Omega}-\dot{\Omega}Jw''-J\ddot{v}''=0 \tag{4}$$

$$EIw^{iv}-mw\Omega^2+2Jw''\Omega^2+2m\dot{v}\Omega+m\ddot{w}+mv\dot{\Omega}-\ddot{\Omega}Jv''-J\ddot{w}''=0 \tag{5}$$

and associated boundary conditions at $x=0$

$$v=w=0,\quad v'=w'=0 \tag{6}$$

and $x=L$

$$EIv'''+Mv\Omega^2+2Jv'\Omega^2+2M\dot{w}\Omega-M\ddot{v}+Mw\dot{\Omega}-\dot{\Omega}Jw'-J\ddot{v}'=-\frac{\varepsilon A_v V_{DC}^2}{2(d_v-v)^2} \tag{7}$$

$$EIw'''+Mw\Omega^2+2Jw'\Omega^2-2M\dot{v}\Omega-M\ddot{w}-Mv\dot{\Omega}-\dot{\Omega}Jv'-J\ddot{w}'=-\frac{\varepsilon A_w (V_{DC}+v_{AC})^2}{2(d_w-w)^2} \tag{8}$$

$$EIv''=0,\quad EIw''=0 \tag{9}$$

It follows from Eqs. (4)–(9) that the drive and sense bending motions are coupled via the base rotation. The angular velocity and acceleration give rise, respectively, to gyroscopic and inertial couplings between the two vibration modes.

Next, we introduce the following set of parameters:

$$\hat{x}=\frac{x}{L},\quad \hat{v}=\frac{v}{d_v},\quad \hat{w}=\frac{w}{d_w},\quad d=\frac{d_v}{d_w},\quad \hat{t}=\tau t,$$

$$\hat{\Omega}=\frac{\Omega}{\tau},\quad \hat{J}=\frac{J}{mL^2},\quad \alpha_v=\frac{\varepsilon A_v L^3}{2EId_v^3},\quad \alpha_w=\frac{\varepsilon A_w L^3}{2EId_w^3},$$

$$M_r=\frac{M}{mL},\quad \tau=\sqrt{\frac{EI}{mL^4}}$$

Then, in nondimensional form, the equations of motion and associated boundary conditions become

$$v^{iv}+c\dot{v}-\Omega^2 v+2J\Omega^2 v''-2\frac{\Omega}{d}\dot{w}+\ddot{v}-\frac{\dot{\Omega}}{d}w-\frac{\dot{\Omega}J}{d}w''-J\ddot{v}''=0 \tag{10}$$

$$w^{iv}+c\dot{w}-\Omega^2 w+2J\Omega^2 w''+2\Omega d\dot{v}+\ddot{w}+\dot{\Omega}dv-\dot{\Omega}dJv''-J\ddot{w}''=0 \tag{11}$$

At $x=0$

$$v=w=0\quad\text{and}\quad v'=w'=0 \tag{12}$$

At $x=1$

$$v'''+M_r\Omega^2 v+2J\Omega^2 v'+2\frac{M_r\Omega}{d}\dot{w}-M_r\ddot{v}+\frac{M_r\dot{\Omega}}{d}w-\frac{J\dot{\Omega}}{d}w'-J\ddot{v}'=-\alpha_v\frac{V_{DC}^2}{(1-v)^2} \tag{13}$$

$$w''' + M_r\Omega^2 w + 2J\Omega^2 w' - 2M_r\Omega\,\mathrm{d}\dot{v} - M_r\ddot{w} - M_r\dot{\Omega}\,\mathrm{d}v - J\dot{\Omega}\,\mathrm{d}v' - J\ddot{w}' = -\alpha_w \frac{(V_{DC}+v_{AC})^2}{(1-w)^2} \tag{14}$$

$$v'' = w'' = 0 \tag{15}$$

where the hats have been dropped for notation convenience and linear damping terms are added to the equations of motion. A common damping coefficient c is used for both directions. We note that the electrostatic forcing terms in Eqs. (13) and (14) are nondimensional and the voltages V_{DC} and v_{AC} are kept dimensional throughout the following analysis.

3. Static deflection

We denote the static deflections in the sense and drive directions by $v_s(x)$ and $w_s(x)$, respectively. The static equilibrium equations are uncoupled and hence are treated separately. In the sense direction, the static configuration of the microbeam is governed by

$$v_s^{\mathrm{iv}} - \Omega^2 v_s + 2J\Omega^2 v''_s = 0 \tag{16}$$

subject to the boundary conditions

$$v_s(0) = 0, \quad v'_s(0) = 0, \quad v''_s(1) = 0$$

$$v'''_s(1) + M_r\Omega^2 v_s(1) + 2J\Omega^2 v'_s(1) = \frac{-\alpha_v V_{DC}^2}{(1-v_s(1))^2} \tag{17}$$

The general solution of Eq. (16) can be expressed as

$$v_s(x) = c_1 e^{a_1 x} + c_2 e^{-a_1 x} + c_3 e^{a_2 x} + c_4 e^{-a_2 x} \tag{18}$$

where

$$a_{1,2} = \sqrt{-J\Omega^2 \pm \sqrt{J^2\Omega^4 + \Omega^2}}$$

The constants c_i are determined by using the boundary conditions in Eq. (17).

We consider a proof mass of thickness 14 μm (M_r=1) and identical sense and drive capacitors with $\mathrm{d}_v = \mathrm{d}_w = 2\,\mu\mathrm{m}$ and $A_w = A_v = 392\,\mu\mathrm{m}^2$. Other dimensions and material properties of the polysilicon microgyroscope are presented in Table 1. This symmetric configuration results in the static deflections in the drive and sense directions being identical $w_s(x)$=$v_s(x)$ for the same DC voltage. This is a desirable outcome since it matches the static deflections on the sense and drive directions, thereby eliminating spurious torsional motions, and matches the natural frequencies in the sense and drive directions, thus amplifying the output motions.

Fig. 2 displays variation of the maximum static deflection $v_s(1)$=v_M in the sense and drive ($w_s(1)$=w_M) directions with the DC voltage V_{DC}. The resulting curve is typical for electrostatic actuators with lower and upper branches of solutions corresponding, respectively, to stable and unstable equilibria of the microbeam. The pull-in voltage is 5.1221 V and the associated deflection (range of travel) is 0.3333.

4. Small motions of the microgyroscope

Microgyroscopes are designed to meet the following performance specifications:

- It must amplify the motions in the sense direction to enable detection and measurement of the output signal.
- It must minimize the voltage requirements in both of the drive and sense directions, thereby minimizing the leakage current and the sensor drift.

Table 1
Microgyroscope parameters.

Symbol	Description	Numerical values
L	Beam length (μm)	400
ρ	Density (kg/m^3)	2300
E	Young's modulus (N/m^2)	160×10^9
m	Mass per unit length (kg/m)	1.803×10^{-8}
M	Tip mass (kg)	7.2128×10^{-12}
b	Beam width (m)	2.8×10^{-6}
h	Beam thickness (m)	2.8×10^{-6}

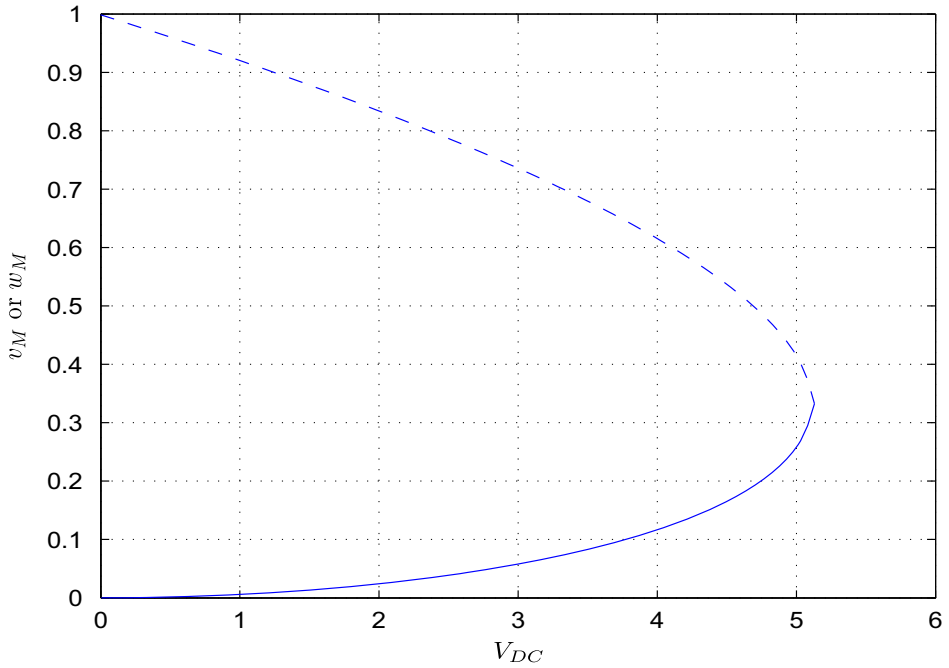

Fig. 2. Maximum deflection versus the applied DC voltage V_{DC} (V) for the drive direction.

We derive an analytical solution of the governing equations of motion to study the dynamic behavior of the gyroscope with a view to optimize its response to meet these design criteria.

The gyroscope is directly excited by a combined DC and AC voltage applied to the proof mass in the drive direction. The AC forcing $v_{AC} = V_{AC}\cos(\Omega_e t)$ is tuned to excite the gyroscope near one of its natural frequencies to satisfy the criteria listed above. We decompose the gyroscope response into static and harmonic components representing motion with the excitation frequency Ω_e; that is,

$$v(x,t) = v_s(x) + (\phi_v(x)e^{i\Omega_e t} + cc) \tag{19}$$

$$w(x,t) = w_s(x) + (\phi_w(x)e^{i\Omega_e t} + cc) \tag{20}$$

where *cc* stands for the complex conjugate of the preceding term. Expanding Eqs. (10)–(15) for small motions around $v_s(x)$ and $w_s(x)$, substituting Eqs. (19) and (20) into the result, using Eqs. (16) and (17), assuming a constant base angular velocity Ω, and dropping the nonlinear terms, we obtain

$$\mathbf{M}_1\boldsymbol{\phi}^{iv} + \mathbf{M}_2\boldsymbol{\phi}'' - \mathbf{M}_3\boldsymbol{\phi} = 0 \tag{21}$$

where

$$\boldsymbol{\phi} = \begin{pmatrix} \phi_v \\ \phi_w \end{pmatrix}$$

$$\mathbf{M}_1 = \begin{pmatrix} 1 & 0 \\ 0 & 1 \end{pmatrix}$$

$$\mathbf{M}_2 = \begin{pmatrix} J\Omega_e^2 + 2J\Omega^2 & 0 \\ 0 & J\Omega_e^2 + 2J\Omega^2 \end{pmatrix}$$

$$\mathbf{M}_3 = \begin{pmatrix} \Omega_e^2 + \Omega^2 - i\Omega_e c & \dfrac{2i\Omega_e\Omega}{d} \\ -2id\Omega_e\Omega & \Omega_e^2 + \Omega^2 - i\Omega_e c \end{pmatrix}$$

$$M_r\phi_v\Omega^2 + 2J\phi'_v\Omega^2 + \frac{2iM_r\phi_w\Omega_e\Omega}{d} + M_r\phi_v\Omega_e^2 + \Omega_e^2 J\phi'_v + \phi'''_v = \frac{2\alpha_v V_{DC}^2}{(1-v_M)^3}\phi_v \quad \text{at } x = 1 \tag{22}$$

$$M_r\phi_w\Omega^2+2J_w\phi'_w\Omega^2-2iM_r\,\mathrm{d}\phi_v\Omega_e\Omega+M_r\phi_w\Omega_e^2+\Omega_e^2J\phi'_w+\phi'''_w=\frac{2\alpha_wV_{DC}^2}{(1-w_M)^3}\phi_w-\frac{2\alpha_wV_{DC}V_{AC}}{(1-w_M)^2}\quad\text{at } x=1 \tag{23}$$

$$\phi''_v(1)=0,\quad \phi''_w(1)=0 \tag{24}$$

$$\phi_v(0)=0,\quad \phi'_v(0)=0,\quad \phi_w(0)=0,\quad \phi'_w(0)=0 \tag{25}$$

where the quality factor Q of the microgyroscope is used to determine the damping coefficient from $c=\omega_0/Q$ and ω_0 is the first natural frequency.

Assuming that the spatial functions $\phi_v(x)$ and $\phi_w(x)$ are of the form

$$\boldsymbol{\phi}(x)=\begin{pmatrix}\phi_{v,i}\\ \phi_{w,i}\end{pmatrix}\mathrm{e}^{s_ix} \tag{26}$$

we obtain the following system of equations:

$$[s_i^4\mathbf{M}_1+s_i^2\mathbf{M}_2-\mathbf{M}_3]\begin{pmatrix}\phi_{v,i}\\ \phi_{w,i}\end{pmatrix}=\begin{pmatrix}0\\0\end{pmatrix} \tag{27}$$

Eq. (27) has nontrivial solution if and only if the determinant of the matrix $[s_i^4\mathbf{M}_1+s_i^2\mathbf{M}_2-\mathbf{M}_3]$ vanishes. Therefore, the general solutions can be written as

$$\boldsymbol{\phi}(x)=\sum_{i=1}^{8}\begin{pmatrix}\phi_{v,i}\\ \phi_{w,i}\end{pmatrix}B_i\mathrm{e}^{s_ix} \tag{28}$$

We substitute Eq. (28) into the boundary conditions (22)–(25) and obtain the linear algebraic system

$$\mathbf{FX}=V \tag{29}$$

in the unknowns $\mathbf{X}^T=[B_1\ B_2\ B_3\ B_4\ B_5\ B_6\ B_7\ B_8]$ where $V^T=\left[0\ 0\ 0\ 0\ 0\ 0\ 0\ -\frac{2\alpha_wV_{DC}V_{AC}}{(1-w_M)^2}\right]$. Eq. (29) is solved for the unknowns B_i. Hence, the beam deflections can be expressed as

$$v(x,t)=v_s(x)+2\left(\sum_{i=1}^{8}\phi_{v,i}B_i\mathrm{e}^{s_ix}\right)\cos\Omega_et \tag{30}$$

$$w(x,t)=w_s(x)+2\left(\sum_{i=1}^{8}\phi_{w,i}B_i\mathrm{e}^{s_ix}\right)\cos\Omega_et \tag{31}$$

We note that the eigenvalue problem can be tackled in a similar way as described above except we replace the excitation frequency Ω_e by the frequency ω, set c=0, and drop the *AC* component in Eq. (23). Therefore, the right-hand side of Eq. (29) becomes equal to zero and then, the natural frequencies are obtained by setting the determinant $|\mathbf{F}(c=0)|$ equal to zero. Fig. 3 shows variation of the first natural frequency with the DC voltage for three values of the tip-mass M. The natural frequency decreases as the electrostatic force increases and approaches zero as pull-in develops. The unactuated (V_{DC}=0 V) natural frequency of the microgyroscope decreases and the curvature of the $\omega-V_{DC}$ curve increases as the tip-mass increases. However, the tip-mass has no effect on the pull-in voltage because it does not contribute to the mechanical restoring force of the beam.

We use the analytical solution given by Eqs. (30) and (31) to calculate the oscillations in both of the drive and sense directions for the three loading cases listed in Table 2. These cases were chosen to examine the effects of the excitation frequency approaching the natural frequency and variation in the common DC voltage applied to the drive and sense electrodes.

4.1. Dynamic amplification

In Fig. 4, we display variation of the microbeam maximum tip displacement with the excitation frequency Ω_e for loading case LC2 and different base rotation velocities. Dynamic amplification can be seen in the peak of the displacement realized in the neighborhood of the natural frequency of the gyroscope. Clearly, the amplitude of the motion in the sense direction increases with the angular speed Ω.

We examine the effect of varying the tip mass on the frequency response curves of loading case LC2. The resulting curves are shown in Figs. 5(a) and (b). Decreasing the tip mass increases the resonance frequency and reduces the amplitudes of the motions along the drive and sense directions. Therefore, considering a larger tip mass may improve the performance of the microgyroscope.

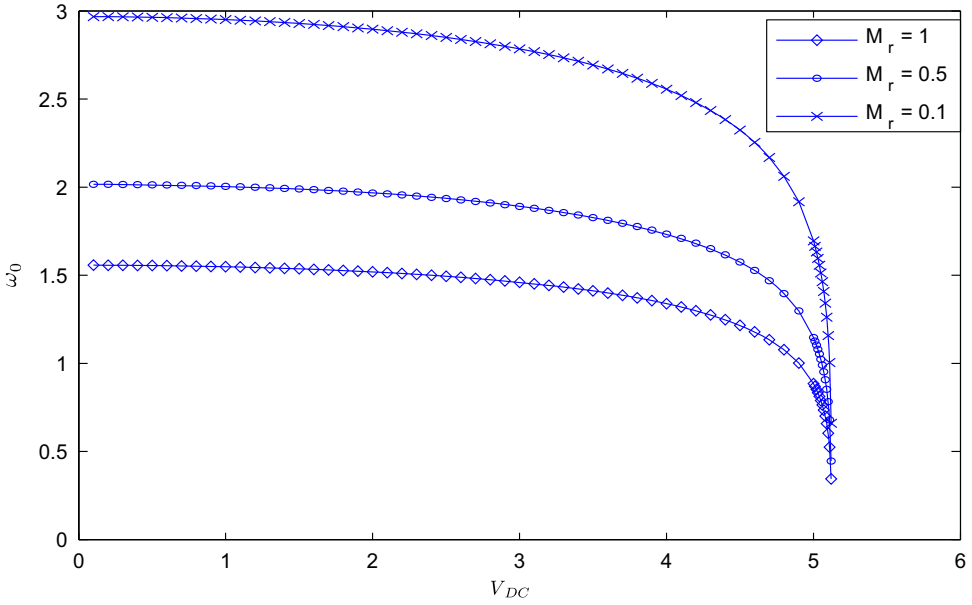

Fig. 3. Variation of the first natural frequency ω_1 with the DC voltage V_{DC} (V) for various values of the tip mass M_r.

Table 2
Loading cases.

Loading case	V_{DC} (V)	V_{AC} (V)	ω_0
LC1	3.8	0.1	1.3717
LC2	4	0.1	1.33882
LC3	4.1	0.1	1.3152

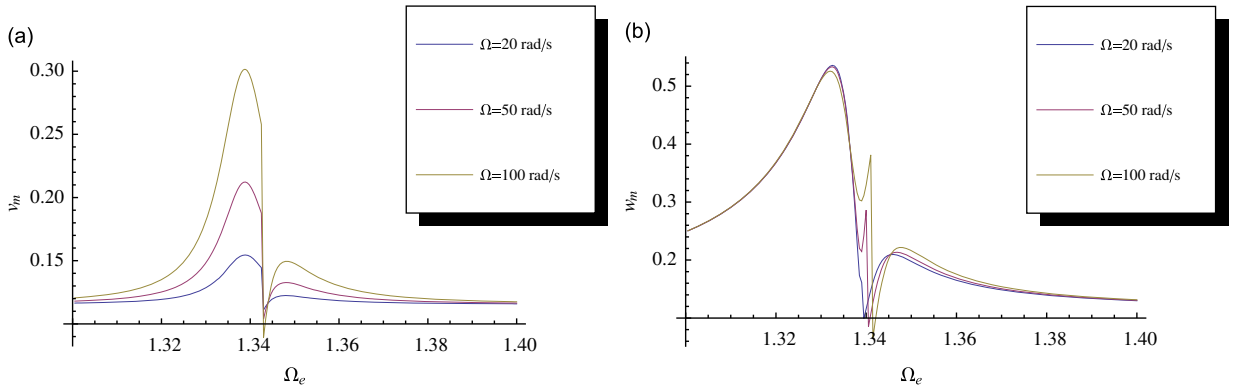

Fig. 4. The frequency-response curves of the gyroscope in the (a) sense and (b) drive directions for different base rotation velocities (LC2, c=0.065).

4.2. Dependance of the system response on the DC voltage

The microbeam is excited with different DC voltages for a constant base rotation velocity ($\Omega = 20\,\mathrm{rad/s}$). Fig. 6 shows variation of the microbeam tip displacement with the DC voltage. As expected, the response amplitudes in both directions increase as the DC voltage increases.

4.3. Calibration curve of the microgyroscope

We present in Fig. 7 variation of the the maximum displacements in the two directions with the rate of rotation about the longitudinal axis of the microgyroscope, for different loadings and an excitation frequency of $\Omega_e = 1.3$. We note that the effect of the base angular speed on the drive direction is insignificant, but its effect on the sense direction is much more

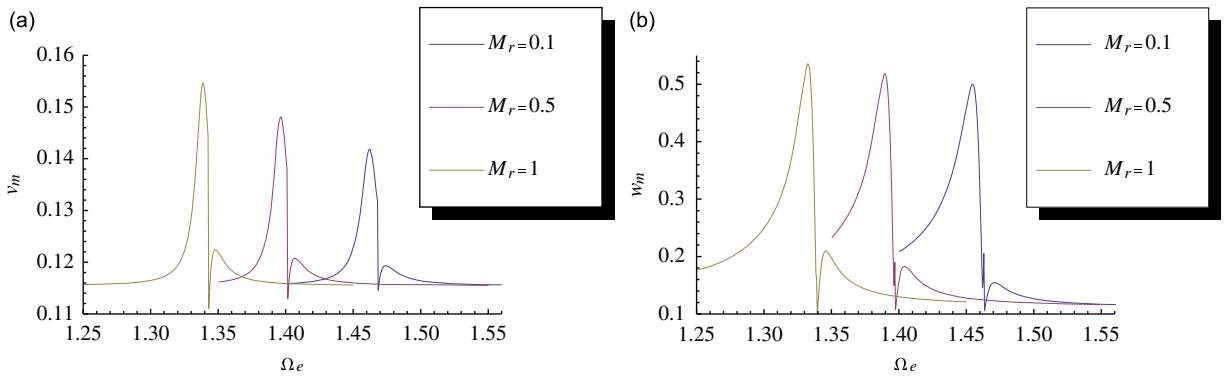

Fig. 5. The frequency-response curves of the gyroscope in the (a) sense and (b) drive directions for different values of the tip mass (LC2, c=0.065).

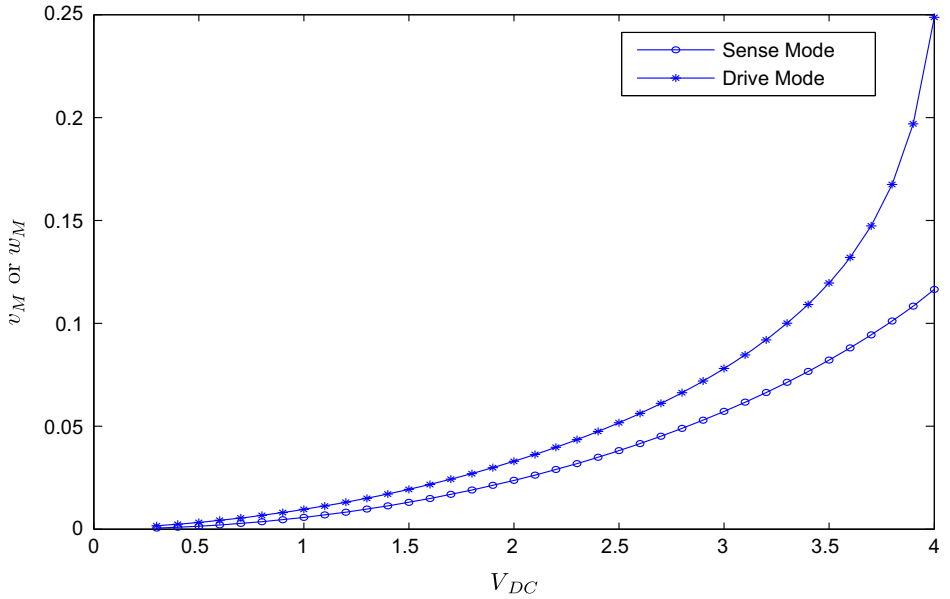

Fig. 6. The gyroscope response as a function of the DC voltage V_{DC} (V) (V_{AC}=0.1 V and $\Omega = 20$ rad/s).

noticeable. The amplitude of motion in the sense direction increases linearly with the angular speed, which is encouraging, because it indicates that capacitive sensing of these motions can produce an easy measure of the angular speed. Moreover, Fig. 7 indicates that the higher the sense direction amplitude is, the more sensitive the microgyroscope becomes. Therefore, by setting the excitation frequency close to the first natural frequency and using an appropriate DC voltage, one can extract the base angular speed from the motion along the sense direction.

To gain more insight into the combined effect of the DC voltage and the base rotation, we generate 3-D plots (see Fig. 8) showing variations of the amplitude of the tip mass oscillations in both of the drive and sense directions with the DC voltage and the base angular speed. These plots reveal that sensitivity of the microgyroscope to the base rotation is more significant as the oscillation amplitude along the sense direction is increased.

5. Conclusion

We consider modeling and performance of a vibrating beam microgyroscope consisting of a rotating cantilever microbeam with a square cross-section and a tip mass at its end. The microbeam is actuated by a pair of DC voltage and AC voltages. Equal DC voltages are applied in the drive and sense directions and a symmetric microstructure is chosen so that the static deflections in both directions are identical for the purpose of avoiding torsional motion, matching their primary resonance, and thus amplifying the output amplitude. The system governing equations are solved analytically to study the relationship between the base rotation and gyroscopic coupling. The effects of the input excitation parameters on the

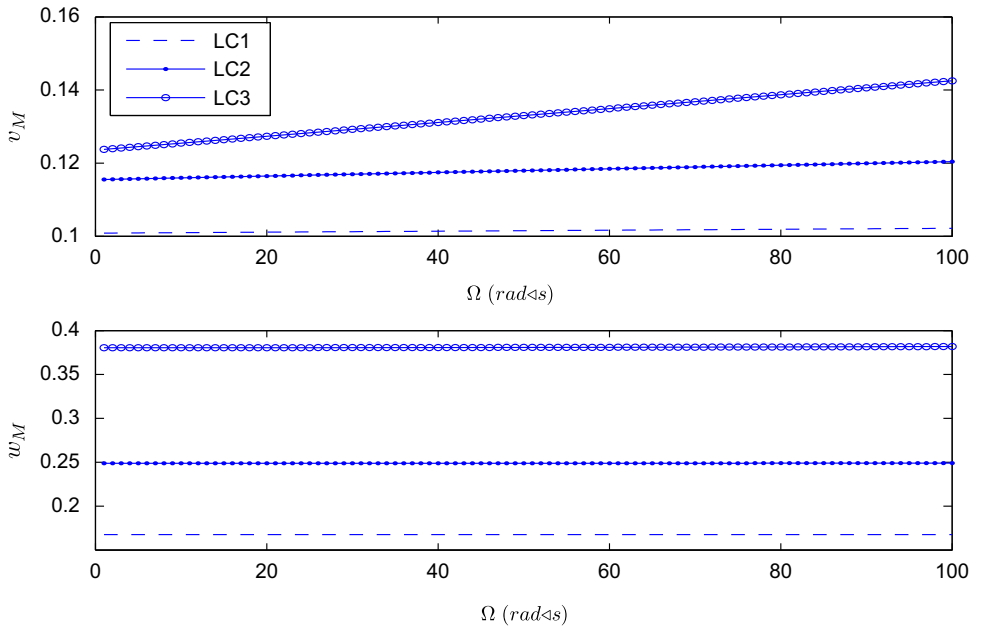

Fig. 7. Variation of the maximum dynamic response with the base rotation: (upper plot) sense mode and (lower plot) drive mode (V_{AC}=0.1 V and $\Omega_e = 1.3$).

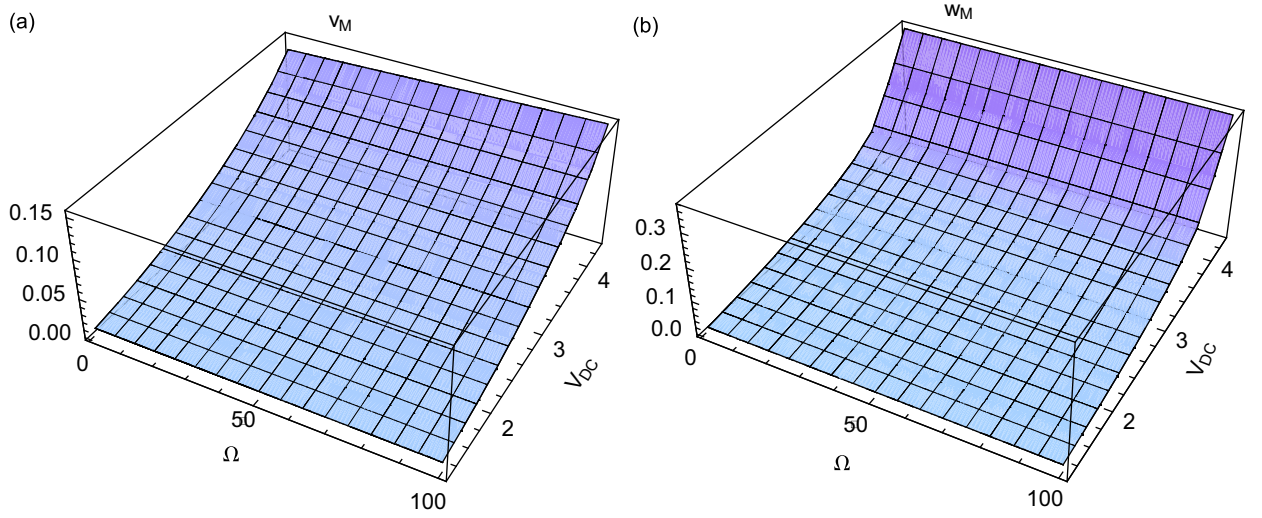

Fig. 8. Effect of the base rotation and the DC voltage V_{DC} (V) on the maximum dynamic response: (a) in the sense direction and (b) in the drive direction ($\Omega_e = 1.3$).

performance of the gyroscope are investigated. We conclude that a large DC voltage (below pull-in) and an excitation frequency close to the fundamental natural frequency enhance sensitivity of the microgyroscope to base rotations.

References

[1] N. Yazdi, F. Ayazi, K. Najafi, Micromachined inertial sensors, *Proceedings of IEEE* (1996) 1640–1659.
[2] S. Sassen, R. Voss, J. Schalk, E. Stenzel, T. Gleissner, R. Gruenberger, F. Neubauer, W. Ficker, W. Kupke, K. Bauer, M. Rose, Tuning fork silicon angular rate sensor with enhanced performance for automative applications, *Sensors and Actuators* 83 (2000) 80–86.
[3] C.B. Williams, C. Shearwood, P.H. Mellor, A.D. Mattingley, M.R. Gibbs, R.B. Yates, Initial fabrication of a micro-induction gyroscope, *Microelectronic Engineering* 30 (1996) 531–534.
[4] M. Kurosawa, Y. Fukuda, M. Tkasaki, T. Huguchi, A surface-acoustic-wave gyro sensor, *Sensors and Actuators* 66 (1998) 33–39.
[5] K. Maenaka, T. Fujita, Y. Konishi, M. Maeda, Analysis of a highly sensitive silicon gyroscope with cantilever beam as vibrating mass, *Sensors and Actuators* 54 (1996) 568–573.
[6] S. Mohite, N. Patil, R. Pratap, Design, modeling and simulation of vibratory micromachined gyroscopes, *Journal of Physics* 34 (2006) 757–763.

[7] A.A. Seshia, Integrated Micromechanical Resonant Sensors for Inertial Measurement Systems, Ph.D. Thesis, University of California, 2002.
[8] C. Acar, A.M. Shkel, Structural design and experimental characterization of torsional micromachined gyroscopes with non-resonant drive mode, *Journal of Micromechanics and Microengineering* 14 (2004) 15–25.
[9] E. Alper, T. Akin, A symmetric surface micromachined gyroscope with decoupled oscillation modes, *Sensors and Actuators A* 97 (2004) 347–358.
[10] Y.S. Hong, J.H. Lee, S.H. Kim, A lateraly driven symmetric micro resonator for gyroscopic applications, *Journal of Micromechanics and Microengineering* 10 (2000) 452–458.
[11] C. Jeong, A study on resonant frequency and Q factor tunings for MEMS vibratory gyroscopes, *Journal of Micromechanics and Microengineering* 14 (2004) 1530–1536.
[12] M. Esmaeili, N. Jalili, M. Durali, Dynamic modeling and performance evaluation of a vibrating beam microgyroscope under general support motion, *Journal of Sound and Vibration* 301 (2007) 146–164.
[13] V. Bhadbhade, N. Jalili, Coupled flexural-torsional vibrations of a piezoelectrically-actuated vibrating beam gyroscope, *Proceedings of 2006 ASME International Mechanical Engineering Conference & Exposition*, Chicago, Il, November 5–10, 2006.
[14] V. Bhadbhade, N. Jalili, S.N. Mahmoodi, A novel piezoelectrically actuated flexural/torsional vibrating beam gyroscope, *Journal of Sound and Vibration* 311 (2008) 1305–1324.
[15] A.H. Nayfeh, P.F. Pai, *Linear and Nonlinear Structural Mechanics*, Wiley-Interscience, New York, 2004.